

An investigation of surface-contacting sensors for the seismic detection of buried landmines

J. S. Martin and G. D. Larson

School of Mechanical Engineering, Georgia Institute of Technology, Atlanta, Georgia 30332-0405

W. R. Scott, Jr.

School of Electrical and Computer Engineering, Georgia Institute of Technology, Atlanta, Georgia 30332-0250

(Received 28 January 2006; revised 21 July 2006; accepted 3 August 2006)

Techniques have been studied for the detection of buried landmines with acoustic/seismic interrogation signals. Much of this work has involved full wave-field imaging from local measurements of ground motion using noncontact sensors. These offer inherent safety for the system operator and accommodate the need to make measurements over rough ground surfaces. The system requirement is, however, only that a sensor does not intrude on the measurement rather than that it not contact the ground. An experimental investigation was conducted into the feasibility of an array of ground-contacting sensors for use in a seismic landmine-detection system that exploits full wave-field imaging. The main considerations in the design of the array sensor were safety, sensitivity, fidelity, reproducibility, and sensor-to-sensor interaction. A relatively simple and inexpensive sensor was demonstrated in an experimental simulation of a landmine-detection system. The sensor, which is suitable for inclusion in a large planar array that could be used for detection confirmation, exerts a safe normal force at the point of contact and enables detection performance comparable to that which could be achieved using noncontact techniques. © 2006 Acoustical Society of America. [DOI: 10.1121/1.2345911]

PACS number(s): 43.40.At, 43.40.Ph, 43.38.Hz, 43.38.Rh [RAS]

Pages: 2676–2685

I. INTRODUCTION

The use of acoustic/seismic signals to detect buried landmines has been studied for well over 30 years.¹ Some of the system concepts that have been explored involve remotely located arrays of ground-contacting seismic sensors and sources to detect mines using pulse-echo techniques.^{2,3} Other system concepts involve local measurement of ground motion at locations, including some directly above buried mines using noncontact sensors.^{4,5} For these systems, the motion is induced by either a remote seismic source or direct air-acoustic coupling at the measurement location. Local measurements offer the advantage that the signal scattered by a landmine is not diminished by geometrical spreading, absorption, or scattering from inhomogeneities in the medium before it can be measured. They also permit the entire surface wave-field to be captured so that data can be processed in the domains of both time and two-dimensional space in order to image the target (concepts that involve direct subsurface vibration measurement have also been proposed in the literature, although these have not been developed to a point of experimental testing⁶). Several noncontact sensor types have been found to be effective in systems based on local measurements. These include laser Doppler vibrometers (LDVs),^{4,7,8} microwave radar-based vibrometers,^{5,9} and ultrasonic vibrometers.^{10,11}

The ground-contacting sensors studied here have been considered in the context of a previously investigated seismic landmine-detection technique.⁵ This technique employs audio-frequency seismic surface waves. These waves are referred to as Rayleigh waves for the sake of brevity, although

they are in fact the lowest order coupled P-SV mode in a vertically heterogeneous medium (i.e., stratified soil). Rayleigh waves interrogate only the near surface layers of soil because they decay exponentially into the medium.¹² These waves are excited by a remotely located source and the full wave-field is measured with a nonintrusive sensor that is scanned to form a synthetic two-dimensional array. The source that is most commonly used is an electrodynamic shaker that is coupled to the ground through a foot designed to preferentially excite Rayleigh waves. Landmine images are formed by post-processing the displacements of the ground's surface measured at many locations. The image processing, which involves spatial and temporal filtering, has been described in previous papers.^{5,13}

In previous work, the receiving array has been synthesized using one or two sensors to scan thousands of measurement locations (typically 2500–5000).⁵ The most significant drawback to this technique is the slow measurement speed that is forced by the synthesis of the receiving array. An obvious path to improve speed is by replacing the synthetic array with a physical array of sensors. Compatibility with this array requires individual sensors with low cost, small physical size, and low power consumption.

A physical array of sensors should yield time savings that are proportional to the number of elements in the array (N) because received signals are simultaneously acquired, and background noise integrated, at many measurement locations. If the array is moved incrementally, movement is N times less frequent for the scanning of a predefined area. In a realistic scenario, N should be an underestimate for the time

savings that can be realized with a physical array in comparison to a synthetic array of identical sensors. This is because the noise field is accurately sampled in time and space and can therefore be filtered more effectively. Nonseismic noise can be removed more effectively by spatial/temporal filters. Seismic noise that passes these filters should constitute a signal of opportunity.

There are many physical configurations that a field-operable landmine-detection system might take. Recent interest has been focused on the development of confirmation systems, which are intended to quickly interrogate a prescribed area that has been identified as a possible landmine location. Here a large physical array of sensors may be used to span an entire region of interest, and the total measurement time should be only that which is required to build a sufficient signal to noise ratio for any individual sensor in the array.

II. ACCELEROMETER-BASED SENSORS

There are many technologies available for measuring surface motion with sensors that contact a surface of interest. These include accelerometers, velocimeters (geophones), seismometers, pressure sensors, and strain sensors. Commercially available accelerometers are an appealing alternative because of their low cost, variety, and ubiquity. Many of these have intrinsic noise densities that are superior to the radar-based sensor used in previous work over most of the frequency range of interest for landmine detection (50–1000 Hz). The radar-based sensor responds to displacement rather than acceleration, so there is a crossover point for signal to noise performance. Many small accelerometers have intrinsic noise density of 10–100 $\mu\text{g}/\sqrt{\text{Hz}}$ in the frequency range of interest. This compares to 1 $\text{nm}/\sqrt{\text{Hz}}$, which was typical of both ultrasonic and radar-based sensors in bench-top testing. Therefore, the crossover for superior noise performance by an accelerometer is in the 50–150 Hz frequency range. Commercially available LDVs advertise intrinsic noise floors of 50 $\text{nm s}^{-1}/\sqrt{\text{Hz}}$. Compared to this, the crossover for superior noise performance by small accelerometers is in the 300–3000 Hz range. Soil is an inconsistent reflector for radar, ultrasound, and laser signals. Measurements using these modalities are usually limited by speckle noise rather than the intrinsic noise of noncontact sensors. Because of this, the crossover frequencies for superior noise performance by accelerometers, which are not susceptible to speckle noise, should be lower for practical purposes than they are for bench-top testing conditions.

An accelerometer is only functional if it is in intimate contact with a vibrating surface. The nature of that contact must satisfy conditions similar to noncontact sensors; the contact must not intrude on the vibration of the ground and it must reasonably couple surface motion to the accelerometer. Additionally, this coupling must be reproducible throughout an array of sensors and when an individual sensor is relocated.

There are three ways in which a ground-contacting sensor might intrude unacceptably on the soil surface in a landmine-detection system. First and most obviously, it

could require a static biasing force that is sufficient to detonate a buried pressure-fused landmine. Anti-personnel (AP) mines impose a more stringent requirement than anti-tank (AT) mines in this regard. Typically pressure-fused AP mines detonate with contact forces of 20–160 N, although some AP mines may be detonated with applied forces as low as 10 N.¹⁴ AT mines detonate with applied forces that are an order of magnitude higher than this. Second, a sensor may load either the ground or a buried mine to alter the surface motion. This is problematic if it degrades the contrast between landmines and background that can be generated by processing the collected data. Thus, some forms of ground loading may be more acceptable than others. Finally, a sensor may scatter the seismic interrogation signal and alter the signals that are received by other sensors in the array. These requirements generally dictate a sensor such as an accelerometer that is small, lightweight, and rigid.

The suitability of an accelerometer for use as a ground-contacting sensor is obvious. However, there are many suspension and packaging schemes that can be used to couple an accelerometer to the ground, and choosing among these is the more difficult question that was addressed in the design of the sensor. This problem was studied through an analysis involving simple lumped-element models for sensor response. The models were validated and several sensor designs were tested in a series of experiments, both in the laboratory and at a realistic field-test site. All of the sensor designs that were modeled and tested were based on commercially available accelerometers.

III. SENSOR DESIGN

The ground-contacting sensor design under consideration can be described as an accelerometer coupled to the ground's surface with a biasing force acting against a tail mass through a spring (as shown in the inset in Fig. 1). This configuration can be represented as a two degree-of-freedom (2-DOF) system.

The sensor head is modeled as a small mass (m_1) that is attached to the ground through a spring and damper (k_0 and η_0) that represent the reactive and resistive components of the ground's input impedance. Previous experiments have shown that the input reactance of the soil at various field sites is dominantly stiffness-like in the frequency range that is of interest for seismic landmine detection.⁵ The stiffness of carefully compacted damp sand, which is a reasonable soil surrogate,^{2,3,15–18} has been measured in the laboratory using an impedance head and found to be approximately 1×10^6 N/m, with a circular contact area of 2 cm^2 that is typical of the prototype sensors. Although viscous damping was assumed, the frequency dependence of the ground-dominated sensor damping was not known and no physical mechanism was assumed for this process. The measured input resistance of the sand in the experimental model can be reasonably modeled in the frequency range of interest as a viscous damper with 76 N/(m/s) damping for a 2 cm^2 contact area. Laboratory measurements were best fit by a frequency dependence that related loss and displacement by a factor of $\omega^{0.84}$, which is reasonably close to the $\omega^{1.0}$ depen-

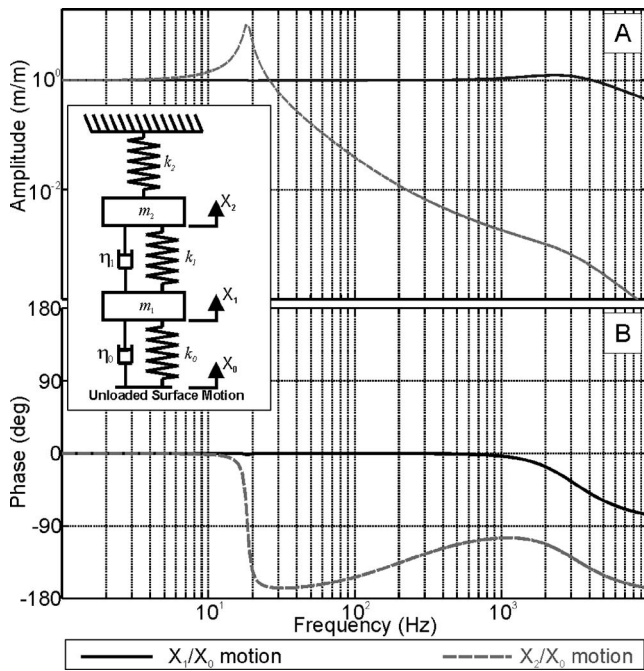


FIG. 1. Modeled response of a gravity-biased ground contacting sensor with a 156 g tail mass (A) amplitude and (B) phase. The model is shown in inset. Here the biasing spring $k_2=0$, foam collar $k_1=2.1 \times 10^3$ N/m, ground $k_0=1 \times 10^6$ N/m, collar damping $\eta_1=1.6$ N/(m/s), ground damping $\eta_0=76$ N/(m/s), head mass $m_1=5.6$ g, and tail mass $m_2=156$ g.

dence that would be expected for viscous damping. Field measurement data of a sufficient quality to perform a similar inversion for other soil types were not available. The tail mass is modeled as a lumped mass (m_2) that is coupled to the sensor head by means of a second spring (k_1). For some of the sensor designs that were examined, the tail mass was coupled to a backing structure through a third spring (k_2), which was used to provide an adjustable biasing force. In selecting parameters for the sensors, k_2 and m_2 were chosen to be sufficient to isolate the tail mass from motion of a complex supporting structure (an automated positioning system) in order to render the device as a whole insensitive to back-plane motion. An accelerometer is an absolute motion rather than a relative motion sensor, but back-plane motion may be coupled into the ground through the accelerometer and thereby affect accelerometer output. This isolation meant that, although the experiments involved a complex supporting structure, the stationary backing assumed in the model is a reasonable approximation. For all of the sensor prototypes, k_1 was selected to isolate m_2 and to be small in comparison to k_0 . In order to minimize intrusion, m_1 was chosen to be as light as possible. The motions of the masses in this model are described by a system of equations as follows:

$$\begin{bmatrix} k_0 + k_1 - m_1\omega^2 + i\omega\eta_0 + i\omega\eta_1 & -k_1 - i\omega\eta_1 \\ -k_1 - i\omega\eta_1 & k_1 + k_2 - m_2\omega^2 - i\omega\eta_1 \end{bmatrix} \times \begin{bmatrix} x_1 \\ x_2 \end{bmatrix} = \begin{bmatrix} (k_0 + i\omega\eta_0)x_0 \\ 0 \end{bmatrix}. \quad (1)$$

This system has two undamped natural frequencies of oscillation that satisfy the equation¹⁹

$$\omega_n^2 = \frac{m_1(k_1 + k_2) + m_2(k_0 + k_1)}{2m_1m_2} \pm \sqrt{\left(\frac{m_1(k_1 + k_2) + m_2(k_0 + k_1)}{4m_1m_2}\right)^2 - \frac{(k_1 + k_2)(k_0 + k_1) - k_1^2}{m_1m_2}}. \quad (2)$$

If components are selected such that $k_0 \gg k_1 \gg k_2$ and $m_2 \gg m_1$, the two resonances are effectively decoupled. The first of these occurs at $\omega_{n1} \approx \sqrt{k_1/m_2}$. This is the resonance of the tail mass on the front spring of the sensor. The second resonance, $\omega_{n2} \approx \sqrt{k_0/m_1}$, is the resonance of the accelerometer mass intimately coupled to the ground's stiffness. The tail mass is effectively stationary for $\omega \gg \omega_{n1}$ where $x_2/x_1 \approx (\omega_{n1}/\omega)(k_1m_1/k_0m_2)$ and the dynamic load on the ground is the mass m_1 . Under these circumstances $x_1 \approx x_0$ (the requirement for sensor fidelity) provided that $\omega \ll \omega_{n2}$. Thus the operational bandwidth of an undamped sensor would be $\sqrt{(k_1/m_2)} \ll \omega \ll \sqrt{(k_0/m_1)}$.

The values of the parameters of the model were determined by direct measurement with the exception of the sensor damping (η_1), which was assumed to be small but non-negligible so that the lower resonance would have a reasonable quality factor. Figure 1 shows the predicted response of a ground-contacting sensor design based on measured parameters, which are indicated in the figure. The lower frequency resonance is seen to have very little effect on the output variable (x_1). This small effect would be diminished further if η_1 were assumed to be larger, but it is not significant even for $\eta_1=0$. For the selected value [$\eta_1=1.6$ N/(m/s)] the quality factor of the lower resonance is 10, which is higher than experimental measurements. The lower resonance frequency for the selected parameters is 18.5 Hz, which is well below the band of interest. The higher resonance, which has a greater impact on the sensor response, occurs at 3 kHz for the selected parameters. The second resonance is heavily damped (the head mass is about twice the mass corresponding to a critically damped system), and therefore has greater effect on the sensor's phase response than on its amplitude response at frequencies of interest. Below 1 kHz, this amounts to less than a 3° phase delay in the sensor response.

Two ground-contacting sensor prototypes that can be modeled by Eq. (1) were designed, built, and tested. These are shown in Fig. 2. The first design [Fig. 2(A)] a spring-biased sensor, was coupled to the backing structure using a long coil spring with a stiffness of 1.3×10^2 N/m. This permitted the normal force on the ground's surface to be easily varied because this biasing force was the sum of the weight of a 40 g tail mass (0.4 N) and the force exerted by the spring's compression. The sensor head weighed 5 g. It was fabricated with a 0.75 g miniature accelerometer (Vibrametrics model VMI9002) encapsulated in rigid foam. The accelerometer sensitivity and noise density were specified by the manufacturer as 100 mV/g and $10 \mu\text{g}/\sqrt{\text{Hz}}$.

The second sensor [Fig. 2(B)] was a modular gravity-biased sensor. It was completely decoupled from its backing structure ($k_2=0$). This sensor was placed on the ground so that it was free standing and then lifted and repositioned

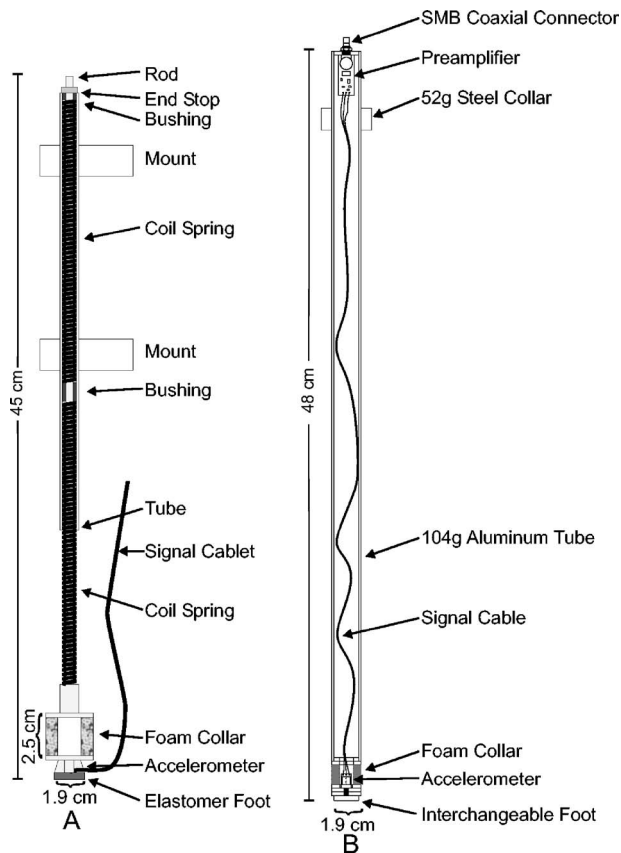


FIG. 2. Two of the vibrometer designs that were tested: (A) a spring-biased sensor and (B) a gravity-biased sensor.

incrementally using a cradle that was not in contact with it during a measurement. The tail mass was a composite made of a 46 cm long 19 mm outer diameter aluminum tube with steel collars attached to it. The long tube permitted the sensor to conform to topography within the array's contact area and the collars allowed for incremental adjustments of the tail mass/biasing force. Each collar was 52 g and the minimum tail mass was 156 g (the mass of the tube with a single collar). The first sensor was one of a kind. The second sensor was built in a quantity of 50 and was designed for use in much larger arrays. The accelerometer for this sensor was selected based primarily on cost and size rather than sensitivity or mass. Here an Analog Devices ADXL103 iMEMs accelerometer was chosen at a cost of less than 1/20th that of the other accelerometers that had been used. This accelerometer had a specified sensitivity and noise density of 1 V/g and 110 $\mu\text{g}/\sqrt{\text{Hz}}$, respectively.

In both sensor designs, the spring represented by k_1 was a section of foam pipe insulation. This permitted the sensor head to move laterally with respect to the tail mass, and to rotate about any axis so that the sensor could be coupled to rough or inclined surfaces and it would not constrain horizontal motion of the ground. This was necessary because the surface motion associated with a Rayleigh wave is elliptical in nature,¹² even though the sensor was only intended to measure its vertical component. The compressive stiffness of the foam springs used in these sensors was measured on a load frame to be 5.4×10^3 N/m for the first design, and

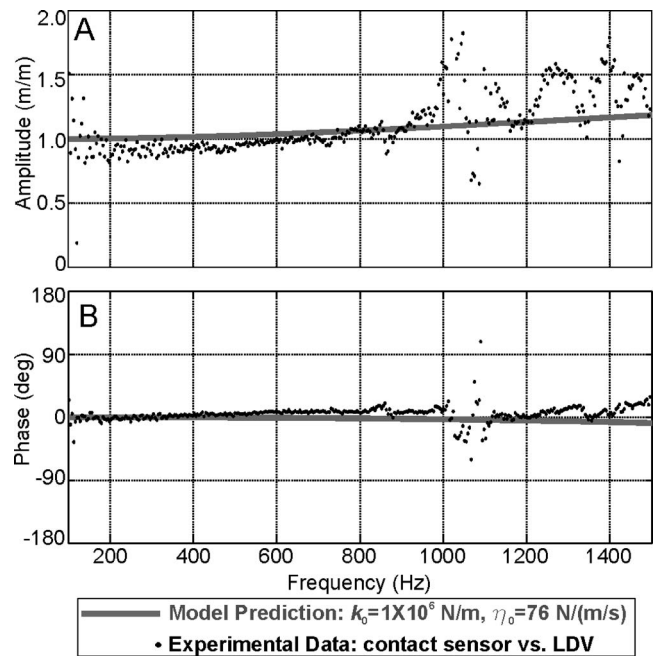


FIG. 3. Modular ground contact sensor transfer function with respect to unloaded ground acceleration (A) amplitude and (B) phase.

2.1×10^3 N/m for the second. In the second design, tubular springs and masses allowed the accelerometers and internal wiring of the sensor to be completely enclosed and weather-proofed.

IV. SENSOR FIDELITY

The fidelity of the ground-contacting sensors described in the previous section was investigated in a series of laboratory experiments using an experimental model filled with damp compacted sand.²⁰ In the first experiment, surface motion was measured using both a ground contacting sensor (a gravity-biased sensor with a total 156 g tail mass) and a commercial LDV in the same location without the sensor present. The sensor and LDV outputs, corrected for the frequency responses of receiving electronics, were used to generate the transfer function that is plotted in Fig. 3, along with the model prediction for this transfer function. The deviations from the predicted behavior are attributable to several sources, including the calibration of the LDV and the accelerometer that were used, the different areas of the surface that are sampled by each sensor, and the nonlinear elasticity of the sand. Below 1 kHz, the sensor deviates from ideal behavior by less than 20% in amplitude and 10° of phase. Most of the structure above 1 kHz is due to the difference between the footprints of the two sensor types, which made their sensitivities vary for each of the different modes of propagation that were present. This is a complex wavefield that includes several modes of surface-guided and bulk waves in addition to the dominant Rayleigh wave. The model assumes that ground is locally reactive and that both sensors would be equally responsive to all components of the incident signal.

Although the sensor has been modeled as a linear 2-DOF system, sand and soils have shown significant non-

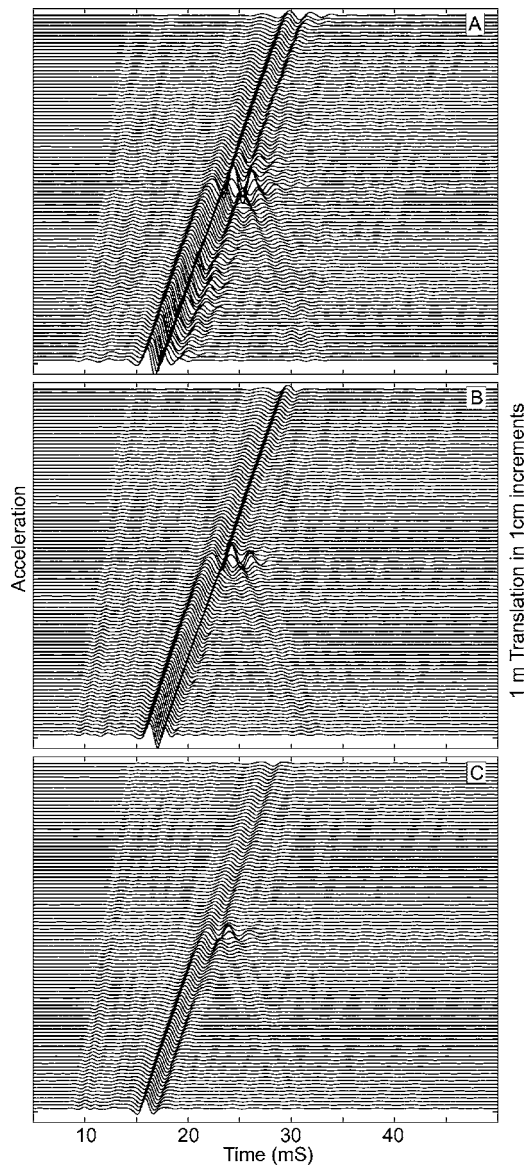


FIG. 4. Accelerations measured from linear scans of a spring-biased sensor away from a seismic source with biasing forces of (A) 1.1 N, (B) 3.6 N, and (C) 11.4 N.

linear behavior.^{21–23} In terms of sensor function, this can manifest itself in a modification of the complex stiffness of the ground at the measurement point (k_0 and η_0) as a function of the applied force at that point. To test this, a series of measurements was made using the spring-biased sensor. The biasing force was progressively increased through the compression of the linear coil spring (k_2), while all the dynamic characteristics of the sensor remained unchanged. The data from these measurements are depicted in the waterfall plots shown in Fig. 4. Each plot here represents 101 measurements made 1 cm apart as the sensor is moved away from the seismic source. The positively sloped diagonal connection of the wavefronts of the largest arrivals in these plots represents the incident Rayleigh wave. The enhanced response 50 cm from the source, and backward propagating waves that originate there, are due to a TS50 AP mine that was buried 1 cm below the surface. If the sensor and medium were perfectly linear, each data set would have been identical aside from the dif-

ferences caused by ambient noise. The differences between these plots, which share a common vertical scale, are therefore an indication of nonlinearity. In Fig. 4(A), a 1.1 N biasing force is seen to be sufficient to detect the incident wave and the presence of the buried mine. There are small differences (other than delays) in these waveforms that are indicative of small changes in the sensor's coupling from point to point. In Figs. 4(B) and 4(C), the biasing force is increased to 3.6 N and 11 N, respectively. Here the reproducibility can be seen to improve with the increased biasing force, but the amplitudes of the measured responses change because of the nonlinearity of the sand. For this effect to pose a problem with respect to landmine detection, it would have to degrade the contrast between the mine and the background in addition to reducing the measured response. This is, of course, a function of the algorithm that is used to convert the measured data into an image. Using imaging techniques that have been reported in previous papers, the data shown in Figs. 4(B) and 4(C) will yield nominally identical contrast after processing.²⁰ With these techniques, the data collected with the 1.1 N biasing force yield a contrast that is degraded by 6–12 dB with regard to the other data sets as a consequence of the reproducibility of the sensor's coupling, rather than the mean fidelity of the measurements. Since this was a synthetic array measurement, the possibility that nonlinearity might adversely affect sensor-to-sensor coupling could not be considered in this analysis.

In another fidelity-related experiment a 20 g sensor head was constructed using a triaxial accelerometer (PCB model W356CA12), with sensitivity and intrinsic noise density comparable to the VMI 9002 accelerometer. This was attached to the spring-biased suspension and used to measure the three components of acceleration on the surface of the damp compacted sand in the experimental model. Figure 5 shows the displacements in the surface normal (Z) and propagation (X) directions that were generated by integration of measurements made 1.5 m from the seismic source. The experiment is configured so that lateral (Y) displacements are negligible in comparison to the other two displacement components. In Fig. 5(A), measurements with a 1.1 N biasing force show that the motion at this location is dominated by two temporally separate pulses. The first of these is characterized by prograde elliptical motion and is consistent with a leaky surface wave (head wave).^{24–26} The second arrival is a larger pulse characterized by retrograde elliptical motion that is consistent with a Rayleigh wave. Although a ground truth for this measurement is not available, the measurement is a reasonable match to measurements made with shallow-buried accelerometers in the same model.²³ The measurement indicates that the sensor has not inordinately constrained in-plane motions at the measurement point. In Fig. 5(B) the same measurement is depicted with a 6.2 N biasing force. It is interesting to note here that the nonlinearities apparent in measurements of the surface normal motion do not equally affect both dominant wave types. The motion associated with the leaky wave, which is mediated by compression, is barely altered by the increased biasing force. The

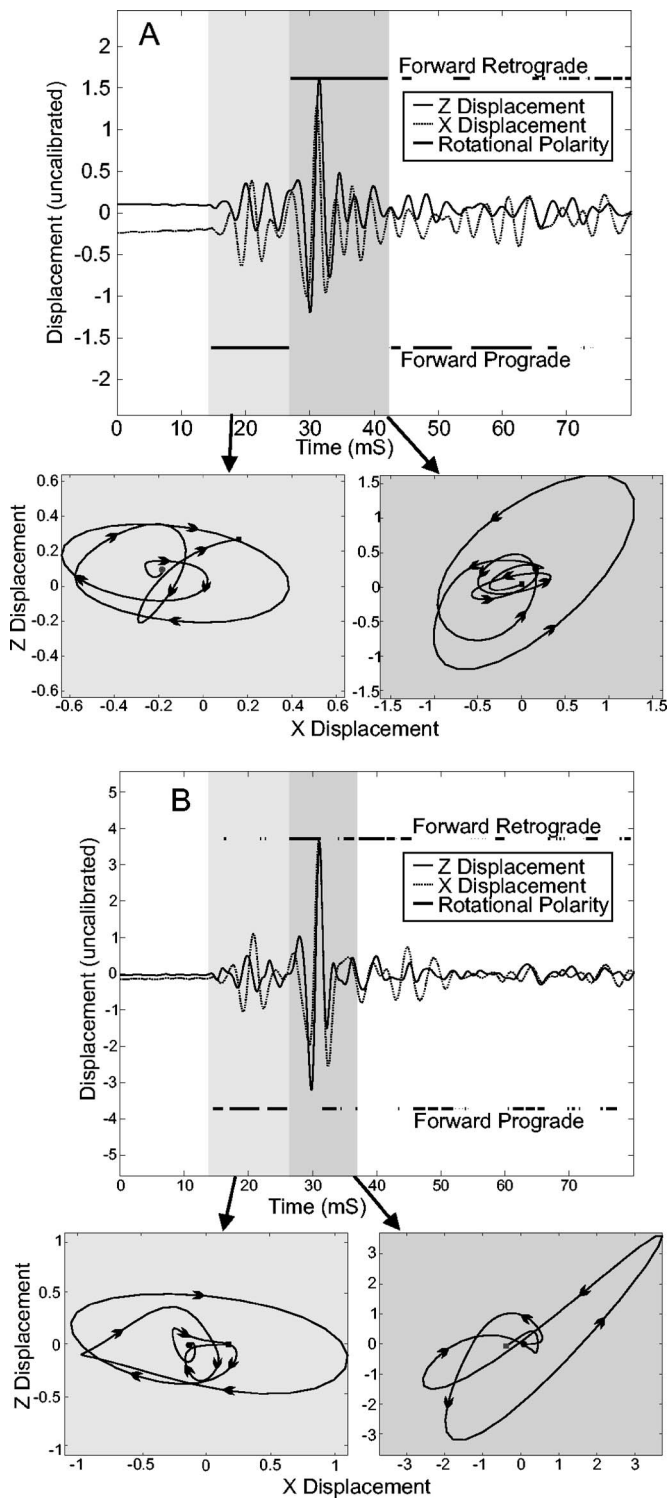


FIG. 5. Hodograms of the displacement measured by a triaxial spring-biased sensor with (A) with a 1.1 N biasing force and (B) with a 6.2 N biasing force.

motion associated with the Rayleigh wave, which is mediated by shear, shows a significant change in both polarity and amplitude at the measurement point.

Although it has not yet been tested experimentally, in-plane displacement information that can be sampled with the ground-contacting sensor, but was not previously available with the radar-based vibrometer, may be exploitable for enhancing the contrast of landmine images. Smith *et al.* have

demonstrated the use of rotational polarity filters to enhance beamforming in a seismic landmine detection system based on pulse echo techniques.³ Although these techniques have not been extended a full wave-field-imaging seismic system, rotational polarity may offer an additional cue to landmine trigger motion.

V. GROUND COUPLING

As mentioned in the previous section, the reproducibility of ground coupling between sensors and measurement locations appears to be a more significant operational problem than the mean fidelity of measurements. Figure 4 clearly demonstrates that reproducibility is directly related to biasing force; however Figs. 4 and 5 demonstrate that there is a cost in terms of fidelity to arbitrarily increasing this. Although the lost fidelity may not pose a problem for landmine imaging (neglecting a possible effect on mutual scattering), increased biasing force is a potential problem in terms of risk to a system operator. For the data shown in Fig. 3, for example, the largest biasing force that was used (11.4 N) could be sufficient to detonate some types of AP landmines, whereas the smallest allowed a safety factor of at least 10.¹⁴ There is also a cost associated with increasing biasing force in a large array, because the backing structure must support the total load associated with the biasing force. A 1000 sensor array requires a structure with lifting capacity of at least 0.1 ton per N of sensor biasing force. For these practical reasons, it is desirable to achieve reproducible coupling with a minimal biasing force.

In the laboratory model, a variety of contact feet and biasing forces were tested in different sensor designs. A subset of three of these contact feet were tested with several biasing forces in a field experiment to see if one of these permitted acceptable point-to-point reproducibility with a lower biasing force than the others. The three designs that were tested were a flat 1.6 cm diameter disk of SorbathaneTM elastomer, a 90° right-circular polycarbonate cone, and a 60° right-circular polycarbonate cone. The three foot designs were tested at a field site located at a government test facility over a simulated dirt road surface, a gravel-covered roadbed, and a grass-covered surface of comparatively loose dry soil. Data acquired using a 60° conical foot with a 5.6 N biasing force on each these surfaces are depicted in Fig. 6. Each of the data sets shown in this figure represents a linear scan over an area with no known buried targets. It is clear from the figure that a surface wave is sensed for each of the conditions. A common vertical scale normalized by the source's driving current is used for all three plots (the absolute acceleration is irrelevant because a pulse-compression scheme was employed for the measurement²⁷). Thus, for a given driving force, which is directly related to drive current for the electrodynamic source, the greatest acceleration response is seen in the gravel roadbed [Fig. 6(B)] and the least response in the grassy area [Fig. 6(C)]. Although the input impedance of the roadbed is higher than the impedance in the grassy area, poor soil consolidation results in more propagation loss and source-coupling nonlinearity in the grass. Similarly, the dirt roadbed [Fig. 6(A)] is a midpoint in

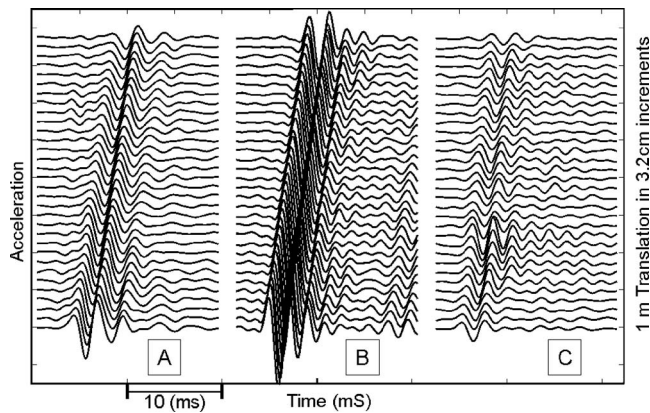


FIG. 6. Windowed waterfall graphs of measured accelerations in a 1 m linear scan away from a seismic at a field site in (A) a dirt roadbed, (B) a gravel roadbed, and (C) a grass-covered area.

terms of consolidation since it contains finer particles than the grass's sandy soil, and larger rounder particles than the crushed granite base of the gravel roadbed. It is clear from the figure that the soft soil and grass pose a greater reproducibility problem than the rough surface and loose stones of the gravel roadbed. All three of the foot designs were tested with biasing forces down to 1.5 N (the minimum permitted by the hardware configuration). This biasing force proved sufficient in the dirt and gravel roadbeds. Unfortunately, the test range that was used did not include either grass-covered landmine burials or grass-covered regions of sifted soil. Given the history of the site, it is likely that both manmade and natural scatterers (tree roots, rocks, etc.) were present in the grassy area. Thus a direct comparison to the other two carefully controlled soil conditions is difficult.

VI. MUTUAL SCATTERING

Although the ground-contacting sensors were designed to be suitable for large physical arrays, these arrays pose a potential problem as compared to noncontact sensor arrays in that the motions of individual sensors may couple through the ground and impede the function of the array. To thoroughly test coupling effects experimentally would require a very large number of sensors or suitable dynamic surrogates. Because these were not available, limited testing of interaction effects was performed using the sensors that were constructed for the field test.

The mutual scattering experiment involved a rectangular array of 10 sensors in the direction of the source (X), and 3 sensors parallel to the incident wavefronts (Y). The spacing of these elements was 3.4 cm \times 10 cm in each direction, respectively. In the experiment, the array was first populated by a single centrally located sensor positioned 1.5 m from the seismic source in the laboratory experimental model. The remaining elements of the array were then populated without disturbing the first sensor. The array's transfer function was constructed as the ratio of the first sensor's response to a seismic incident signal within the array to that sensor's response when the other array locations were empty. This transfer function is plotted in Fig. 7. From the figure, it is apparent that between 150 Hz and 1100 Hz the surrounding

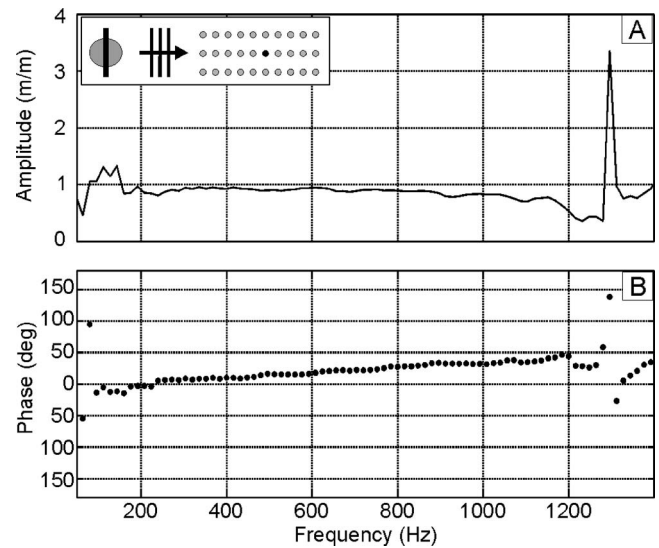


FIG. 7. Transfer function of a single ground-contacting sensor in rectangular array/alone (A) amplitude and (B) Phase. Source and sensor locations are shown in inset.

array reduces the output of the sensor slightly (≤ 3 dB). A small amplification below 150 Hz appears to be indicative of changes in the background noise, which was produced by machinery in adjoining laboratories. The spike at ~ 1300 Hz is due to a slight downward shift in a spectral null that was caused by interference of the various modes and paths comprising the received signal when the array was populated. The phase of the transfer function shows that there is a delay (linear frequency-phase relationship) between the two measurements. This delay is approximately 14 μ s, with the sensor-in-array output leading that of the lone sensor. A plausible explanation for this is that there is a local increase in the shear modulus of the sand around each sensor that is caused by the applied biasing force. This is consistent with the observed reduction in sensor response that results from increasing the biasing force. If this delay is equated with a change in propagation speed over the portion of the array that lies between the sensor and the source (5 sensors spanning 17 cm), it predicts that the array increases the incident signal's mean propagation speed (dominantly the Rayleigh wave speed, although other modes are present) by approximately 1% over its extent. If the problem is viewed as a one-dimensional transmission line, the propagation speed change can only account for a 0.5% amplitude reduction in signal level. More likely explanations for the reduced sensor output observed following the introduction of the array are that it is due to loss in the foam springs of the intervening sensors, or due to shadowing.

VII. LANDMINE IMAGING

The field experiment that was done to evaluate sensor performance involved a linear array of 32 gravity-biased sensors with 156 g tail masses spaced 3.2 cm apart. The array was scanned in 32 steps perpendicular to its alignment to form a semisynthetic 1 m² planar array. Figure 8 shows the experimental setup that was used at the field site. The seismic source was oriented both for a broadside and for an

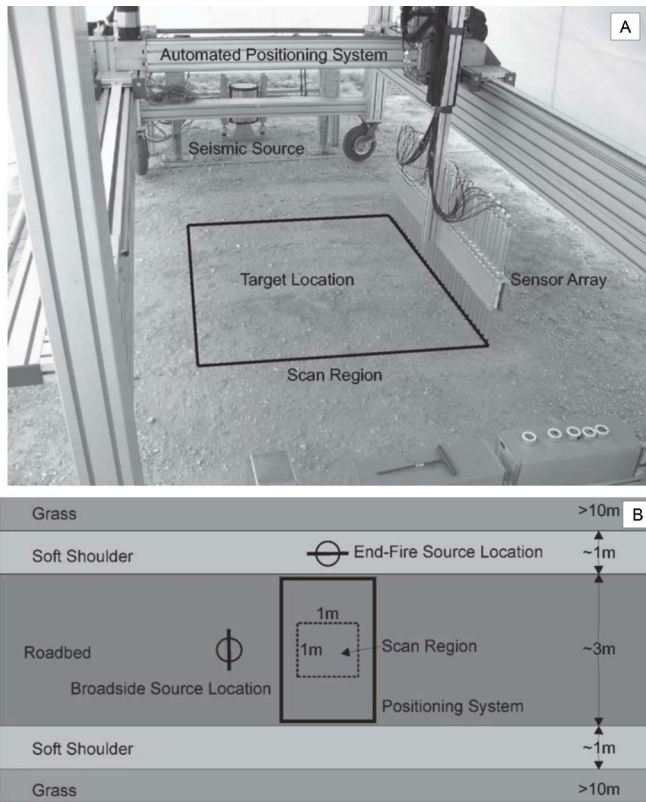


FIG. 8. Configuration of field experiment: (A) photograph of system on simulated dirt roadbed and (B) layout of experiment at field site.

end-fire illumination of the linear array. Although this should have provided insight into mutual scattering effects, the roadbeds at the test site exhibited significant horizontal anisotropy, which was the dominant difference between the two incident signal aspects. There was a horizontal gradient in surface wave speed of the roadbed, which slowed near both shoulders. For all of the measurements, the linear array was located perpendicular to the roadbed. Thus, the end-fire measurements required the source to be located in the low-speed region.

Processed images from the field measurements for various landmine types, road conditions, and propagation directions are depicted in Figs. 9 and 10. Figure 9 contains images formed with data collected in a dirt roadbed, and Fig. 10 shows images from an adjoining gravel roadbed. The targets were all AT landmines or landmine simulants that had been well-weathered in place prior to the experiment to ensure that none of the detections were tied to trenching effects. The array was located to place targets in the approximate center of the scan region, but some of the targets' locations were not well-known and these are offset slightly. Collectively, the images demonstrate sufficient reproducibility and fidelity across the array for the conditions that were examined. This is remarkable given the size of the largest stones on the gravel roadbed, which was comparable to the diameter of the sensor. At many measurement locations, sensors were in contact with a single stone, and sensors frequently sat at steep angles of repose atop these stones. Due to the anisotropy of the roadbeds, there are obvious differences in the images

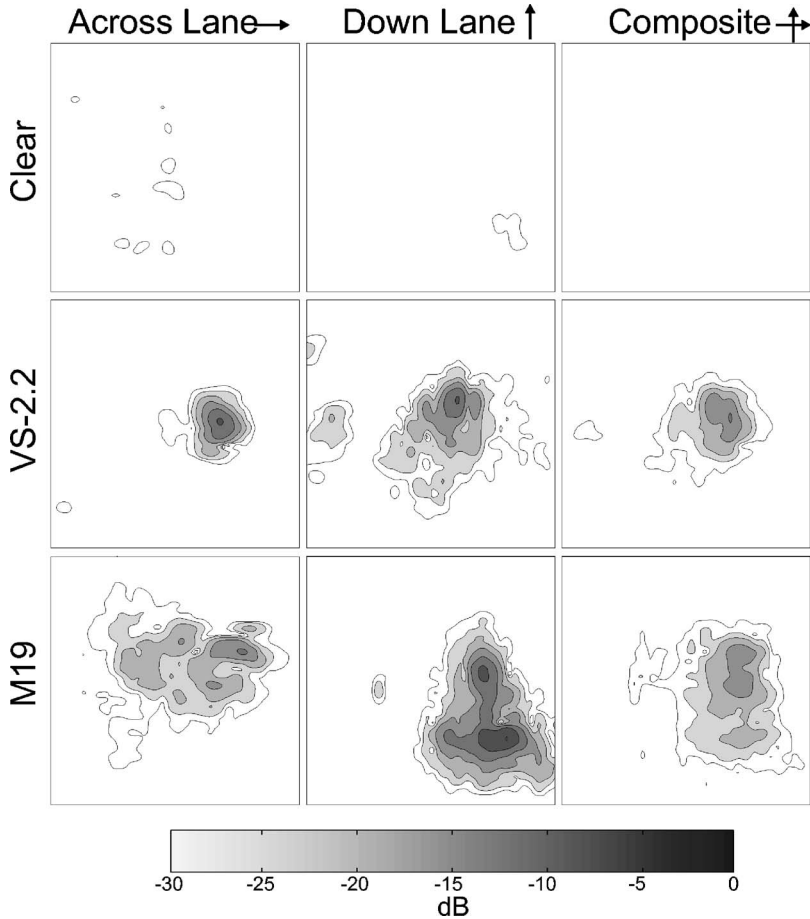


FIG. 9. Images of AT landmines in a dirt roadbed at the field test site: Rows represent mine types as labeled and columns represent the propagation direction of the interrogation signal with the roadbed as labeled. Color is scaled to the maximum pixel value (M19, down lane).

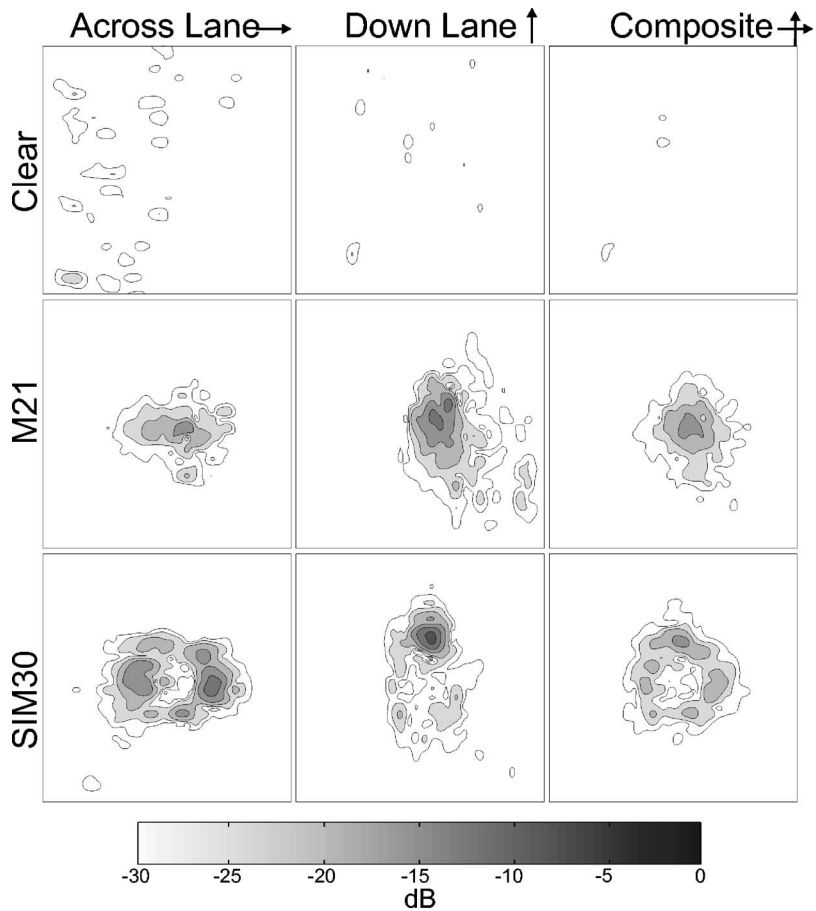


FIG. 10. Images of AT landmines in a gravel roadbed at the field-test site: Rows represent mine types as labeled and columns represent the propagation direction of the interrogation signal with respect to the roadbed as labeled. Color is scaled to the maximum pixel value from Fig. 9.

formed using different source locations in otherwise identical scans. Images formed from incident seismic signals that propagated perpendicular to the road bed (shown in the first columns of Figs. 9 and 10) generally show less background contrast than those that were formed from incident signals propagating parallel to it (shown in the middle columns of the figures).

All of the data were processed with an imaging algorithm that had been developed and refined for use with synthetic array measurements employing a radar-based sensor. The algorithm does not account for the spreading and attenuation of the incident signal and is therefore more sensitive to objects closer to the source. The algorithm may also smear large targets in the direction of the source. Thus, clutter in the original data, regardless of its cause, will produce image clutter that is dependent on its location relative to both the seismic source and the buried target.

In a system designed to search progressively through a region, the deficiencies of the imaging algorithm would need to be accepted or remedied through the use of alternative signal processing techniques. The confirmation-system application that was previously discussed permits this problem to be addressed through a reconfiguration of system hardware. Since the region to be inspected has been prescribed on all sides for the confirmation system, it may be illuminated from any direction or from multiple directions. Each different look direction will result in a shift of the artifact-dominated contributions to the background, while the location of buried objects will be fixed in space. This is apparent in the corre-

sponding pairs of images in the first and second columns of Figs. 9 and 10. It should therefore be possible to improve resolution in the resulting image by combining data from several look directions. This can be done without adding to measurement time by exploiting spread spectrum techniques and simultaneously exciting all of the sources with coded signals.^{28,29}

The potential to improve image resolution and contrast with multiple look directions was tested with data collected in the field experiment because the laboratory model is not large enough to permit this sort of experiment. The images shown in the first two columns of Figs. 9 and 10 were combined to form the corresponding images in the third column. The images were combined by taking the square root of the product of corresponding image pixel values. The combined images show better spatial resolution than either of their precedents. The reduction in the overall background (~ 3 dB) is not as striking as the reduction of the peak levels measured over some of the landmines. Improved spatial resolution is particularly apparent for the data collected over the SIM30 landmine simulant in the gravel roadbed. Here the combined image clearly outlines the perimeter of the simulant. Any number of data sets collected using different source locations could be integrated in this way, although there are other schemes that can be used to combine these data sets, which may offer advantages over the chosen technique.

VIII. CONCLUSIONS

Ground contacting sensors have been designed, built and tested for use in a seismic landmine-detection system. The sensor design that has been considered is not as easily scanned as noncontacting sensors are, but is suited to the incremental motion of a detection-confirmation system. Its deployment requires that a psychological barrier to touching the ground above a buried mine be overcome. Experimental testing indicates that the current design is capable of meeting reasonable requirements for cost, sensitivity, fidelity, nonintrusion, reproducibility of ground coupling, and large-array compatibility. Measurements that have been conducted with these sensors in both a laboratory model and at a realistic outdoor site reveal that the most significant deviations from ideal behavior are attributable to the nonlinearity of the soil that a sensor contacts.

ACKNOWLEDGMENTS

This work was supported by the Office of Naval Research under Contract No. N00014-04-1-0613 and by the U.S. Army RDECOM CERDEC Night Vision and Electronic Sensors Directorate under Contract No. DAAB07-03-D-C213-0006.

- ¹J. C. Cook and J. J. Wormser, "Semi-remote acoustic, electric and thermal sensing of small buried nonmetallic objects," *IEEE Trans. Geosci. Electron.* **GE-11**(3), 135–152 (1973).
- ²"Feasibility of acoustic landmine detection: Final technical report," BBN Technical Report No. 7677, May 1992.
- ³E. Smith, P. S. Wilson, F. W. Bacon, J. F. Manning, J. A. Behrens, and T. G. Muir, "Measurement and localization of interface wave reflections from a buried target," *J. Acoust. Soc. Am.* **103**, 2333–2343 (1998).
- ⁴J. M. Sabatier and N. Xiang, "An investigation of acoustic-to-seismic coupling to detect buried antitank landmines," *IEEE Trans. Geosci. Remote Sens.* **39**, 1146–1154 (2001).
- ⁵W. R. Scott, Jr., J. S. Martin, and G. D. Larson, "Experimental model for a seismic landmine detection system," *IEEE Trans. Geosci. Remote Sens.* **39**, 1155–1164 (2001).
- ⁶K. Sarabandi and D. E. Lawrence, "Acoustic and electromagnetic wave interaction: Estimation of Doppler spectrum from an acoustically vibrated metallic circular cylinder," *IEEE Trans. Antennas Propag.* **51**, 1499–1507 (2003).
- ⁷N. Xiang and J. M. Sabatier, "An experimental study on antipersonnel landmine detection using acoustic-to-seismic coupling," *J. Acoust. Soc. Am.* **113**, 1333–1341 (2003).
- ⁸D. Donskoy, A. Ekimov, N. Sedunov, and M. Tsionskiy, "Nonlinear seismo-acoustic land mine detection and discrimination," *J. Acoust. Soc. Am.* **111**, 2705–2714 (2002).
- ⁹S. H. Lee and W. R. Scott, Jr., "A focused radar antenna for use in seismic mine detection systems," *Radio Sci.* **39** (2004).
- ¹⁰J. S. Martin, D. J. Fenneman, F. Codron, P. H. Rogers, W. R. Scott, G. D. Larson, and G. S. McCall, "Ultrasonic displacement sensor for the seismic detection of buried land mines," in *Proceeding SPIE: 2002 Annual International Symposium on Aerospace/Defense Sensing, Simulation, and Controls*, Orlando, FL, April 2002, Vol. **4742**, pp. 606–616.
- ¹¹A. G. Petculescu and J. M. Sabatier, "Air-coupled ultrasonic sensing of grass-covered vibrating surfaces; qualitative comparisons with laser Doppler vibrometry," *J. Acoust. Soc. Am.* **115**, 1557–1564 (2004).
- ¹²J. D. Achenbach, *Wave Propagation in Elastic Solids*, 7th ed. (Elsevier Science, New York, 1993), pp. 187–194.
- ¹³A. Behboodian, W. R. Scott, Jr., and J. H. McClellan, "Signal processing of elastic surface waves for localizing buried land mines," in *Proceedings of the 33rd Assilomar Conference on Signals, Systems, and Computers*, Pacific Grove, CA, **2 pt.2**, pp. 827–830 (1999).
- ¹⁴*Jane's Mines and Mine Clearance*, 9th ed. edited by C. King (Janes Information Group, Alexandria, VA, 2004), pp. 63–463, and 195, 199, 265, 269, and 357 contain salient examples of pressure-fused AP mine triggering forces.
- ¹⁵R. Bachrach and A. Nur, "High-resolution shallow-seismic experiments in sand, Part I: Water table, fluid flow, and saturation," *Geophysics* **63**(4), 1225–1233 (1988).
- ¹⁶R. Bachrach, J. Dvorkin, and A. Nur, "High-resolution shallow-seismic experiments in sand, Part II: Velocities in shallow unconsolidated sand," *Geophysics* **63**(4), 1234–1240 (1998).
- ¹⁷M. Westebbe, J. F. Bohme, H. Krummel, and M. B. Matthews, "Model fitting and testing in near surface seismics using maximum likelihood in frequency domain," in *Conference Record 32rd Assilomar Conference Signals, Systems, and Computers*, Pacific Grove, CA, Vol. 2, pp. 1311–1315 (1998).
- ¹⁸J. M. Sabatier, H. E. Bass, L. N. Bolen, and K. Attenborough, "Acoustically induced seismic waves," *J. Acoust. Soc. Am.* **80**(2), 646–649 (1986).
- ¹⁹L. Meirovitch, *Elements of Vibration Analysis*, 2nd ed. (McGraw-Hill, New York, 1986), pp. 107–116.
- ²⁰J. S. Martin, G. D. Larson, and W. R. Scott, Jr., "Surface-contacting vibrometers for seismic landmine detection," in *Proceedings of SPIE: 2005 Annual International Symposium on Aerospace/Defense Sensing Simulation, and Controls*, Orlando, FL, April, 2005, Vol. **5794**, pp. 590–600.
- ²¹J. C. Santamarina, K. A. Klein, and M. A. Fam, *Soils and Waves: Particulate Materials Behavior, Characterization, and Process Monitoring* (Wiley, Chichester, England, 2001), pp. 103–115 and 246–247.
- ²²M. S. Korman and J. M. Sabatier, "Nonlinear acoustic techniques for landmine detection," *J. Acoust. Soc. Am.* **116**, pp. 3354–3369 (2004).
- ²³G. D. Larson, J. S. Martin, P. H. Rogers, W. R. Scott, and G. S. McCall, "Impact of nonlinear effects on high-frequency seismic landmine detection," in *Proceedings of the 5th International Symposium on Technology and the Mine Problem*, April 22–25 2002, Monterey California (<http://www.hdic.imu.edu/dtif/Conferences/Monterev2/LAND/MARTIN.PDF>).
- ²⁴L. Tsang, "Time-harmonic solution of the elastic head wave problem incorporating the influence of Rayleigh poles," *J. Acoust. Soc. Am.* **63**(5), 1302–1309 (1978).
- ²⁵C. T. Schröder and W. R. Scott, Jr., "On the complex conjugate roots of the Rayleigh equation: The leaky surface wave," *J. Acoust. Soc. Am.* **110**(6), 2867–2877 (2001).
- ²⁶J. G. Harris and J. D. Achenbach, Comment on "On the complex conjugate roots of the Rayleigh equation: The leaky surface wave," *J. Acoust. Soc. Am.* **112**(5), 1747–1748 (2002).
- ²⁷J. S. Martin, W. R. Scott, G. D. Larson, P. H. Rogers, and G. S. McCall II, "Probing signal design for seismic landmine detection," in *Proceedings of the SPIE: 2004 Annual International Symposium on Aerospace/Defense Sensing, Simulation, and Controls*, Orlando, FL, April 2004, Vol. **5415**, pp. 133–144.
- ²⁸H. L. Van Trees, *Detection, Estimation, and Modulation Theory Part I* (Wiley, New York, 1968), pp. 257–287 and 381–386.
- ²⁹A. J. Viterbi, *CDMA, Principles of Spread Spectrum Communication* (Addison-Wesley, Reading, MA, 1995), pp. 4–51.